

# Impact of spring phenology variation on GPP and its lag feedback for winter wheat over the North China Plain



Linghui Guo<sup>a</sup>, Jiangbo Gao<sup>b,\*</sup>, Shouchen Ma<sup>a,\*\*</sup>, Qing Chang<sup>c</sup>, Linlin Zhang<sup>b</sup>, Suxian Wang<sup>d</sup>, Youfeng Zou<sup>a</sup>, Shaohong Wu<sup>b</sup>, Xiangming Xiao<sup>c</sup>

<sup>a</sup> School of Surveying and Land Information Engineering, Henan Polytechnic University, Jiaozuo 454000, China

<sup>b</sup> Key Laboratory of Land Surface Pattern and Simulation, Institute of Geographic Sciences and Natural Resources Research, Chinese Academy of Sciences, 11A Datun Rd., Beijing 100101, China

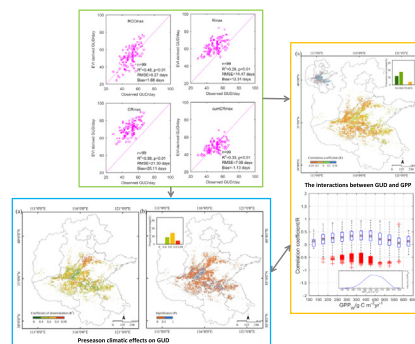
<sup>c</sup> Department of Microbiology and Plant Biology, University of Oklahoma, Norman, OK 73019, USA

<sup>d</sup> Emergency Management School, Henan Polytechnic University, Jiaozuo 454000, China

## HIGHLIGHTS

- The RCCmax algorithm has good performance in capturing the spatiotemporal variation of winter wheat GUD over the NCP.
- Considering the non-identical lag time effects of hydrothermal factors is of importance for revealing GUD response.
- Sensitivity of GUD to changing climate could be amplified by the positive feedback effect from GPP variation.

## GRAPHICAL ABSTRACT



## ARTICLE INFO

### Article history:

Received 20 October 2019

Received in revised form 17 March 2020

Accepted 29 March 2020

Available online 1 April 2020

Editor: Zhibin Sun

### Keywords:

North China Plain

Winter wheat

Spring phenology

Plant productivity

Hydrothermal variation

## ABSTRACT

Spring green-up date (GUD) is a sensitive indicator of climate change, and of great significance to winter wheat production. However, our knowledge of the chain relationships among them is relatively weak. In this study, based on 8-day Enhanced Vegetation Index (EVI) data from Moderate Resolution Imaging Spectroradiometer (MODIS) from 2001 to 2015, we first assessed the performance of four algorithms for extracting winter wheat GUD in the North China Plain (NCP). A multiple linear regression model was then established to quantitatively determine the contributions of the time lag effects of hydrothermal variation on GUD. We further investigated the interactions between GUD and gross primary production (GPP) comprehensively. Our results showed that the rate of change in curvature algorithm (RCCmax) had better performance in capturing the spatiotemporal variation of winter wheat GUD relative to the other three methods (Kmax, CRmax, and cumCRmax). Regarding the non-identical lag time effects of hydrothermal factors, hydrothermal variations could explain winter wheat GUD variations for 82.05% of all pixels, 36.78% higher than that without considering the time lag effects. Variation in GUD negatively correlated with winter wheat GPP after green up in most parts of the NCP, significantly in 35.75% of all pixels with a mean rate of  $1.89 \text{ g C m}^{-2} \text{ yr}^{-1} \text{ day}^{-1}$ . Meanwhile, winter wheat GPP exerted a strongly positive feedback on GUD in >82.42% of all pixels (significant in 28.01% of all pixels), characterized by

\* Correspondence to: J. Gao, Key Laboratory of Land Surface Pattern and Simulation, Institute of Geographic Sciences and Natural Resources Research, Chinese Academy of Sciences, Beijing 100101, China.

\*\* Correspondence to: S. Ma, School of Surveying and Land Information Engineering, Henan Polytechnic University, Jiaozuo 454000, China.  
E-mail addresses: [gaojiangbo@igsrr.ac.cn](mailto:gaojiangbo@igsrr.ac.cn) (J. Gao), [mashouchen@hpu.edu.cn](mailto:mashouchen@hpu.edu.cn) (S. Ma).

a humped-shape pattern along the long-term average plant productivity. This finding highlights the complex interaction between spring phenology and plant productivity, and also suggests the importance of pre-season climate factors on spring phenology.

© 2020 Elsevier B.V. All rights reserved.

## 1. Introduction

Spring green-up date (GUD) refers to the periodic timing of recurring biological cycles, and is considered extremely sensitive to climate change (Schwartz et al., 2006; Cong et al., 2012). Over recent decades, the advancement of GUD has been examined broadly across North America, Europe and East Asia using in situ observations (Wolfe et al., 2005; Fu et al., 2014; Ge et al., 2015), satellite data (Jeong et al., 2011; Park et al., 2016) and phenological models (Han et al., 2018; Liu et al., 2018a) in the context of climate change. Although the predominant processes affecting GUD vary substantially among different regions (Jeong et al., 2011; Piao et al., 2019), variations in GUD over the Northern Hemisphere could be mostly attributable to the pre-season temperature and precipitation (Jeong et al., 2011; Cong et al., 2013; Fu et al., 2015). For example, a 1 °C increase in pre-season daytime temperature would advance leaf unfolding dates by 4.3–4.7 in the United States and Europe (Piao et al., 2015), and an increase in 10 mm precipitation may advance GUD at least 1 day in the southwestern plateau (Shen et al., 2015). However, most of these studies focused mainly on natural ecosystems (Jeong et al., 2011; Shen et al., 2014; Fu et al., 2015; Shen et al., 2016). Although earlier researchers have presented several case studies on the spatiotemporal pattern of crop GUD and diagnosed the responses of GUD to pre-season hydrothermal variations (Liu et al., 2017; Wang et al., 2017b; Guo et al., 2019), we have not yet acquired an explicit understanding of the combined effect of pre-season temperature and precipitation variations in regulating GUD dynamics due to the non-uniform lag time effects of these factors on GUD variation emphasized in recent studies (Shen et al., 2016; Rossi and Isabel, 2017; Xia et al., 2018).

The importance of GUD shifts on annual gross primary production (GPP) variability is evident (Piao et al., 2007; Richardson et al., 2010). Combined with photosynthetic capacity and the end of the growing season, it successfully determined vegetation primary production, explaining >90% of the variation in annual GPP in most areas of North America (Xia et al., 2015; Zhou et al., 2017). However, the relationships between GUD and annual GPP variability were heavily dependent on locations and vegetation types (Zhou et al., 2016). For instance, GUD positively contributed to annual GPP variability for 87.9% of North America, whereas its contribution was negative in most of the northern North American plains (Zhou et al., 2017). Hence, in view of the different responses to GUD, the possible effects of GUD on the variability of GPP across regional ecosystems should be further investigated, which is of great significance to systematically understand the biological mechanisms involved in how vegetation respond to climate change. Furthermore, researchers have suggested that any change in GPP, as the largest carbon flux, would greatly affect the ecosystem carbon balance and thus feeds back to vegetation growth (Badgley et al., 2017; He et al., 2018a; Yao et al., 2018). Nevertheless, to our knowledge, whether GUD-induced changes in plant productivity can in turn feed back to GUD has not been investigated widely.

Compared with in situ observation, remote sensing provides a compensatory and effective way to monitor large-scale changes in vegetation GUD (Cong et al., 2012; Piao et al., 2019). However, at present, considerable uncertainties remain in GUD derived from satellite data. First, it has been suggested that the variation in satellite-derived GUD differs dramatically among different satellite datasets due to bandwidths, sensors and temporal resolutions (Ahl et al., 2006; Zeng et al., 2011; Zhang et al., 2013; Shen et al., 2014; Liu et al., 2017). Furthermore,

even when using the same dataset, significant variations in estimated GUD still occur. This discrepancy may probably relate to the filter function and extraction algorithms (White et al., 2009; Cong et al., 2013; Shen et al., 2014). By comparing across an ensemble of 10 methods, White et al. (2009) found that GUD estimations for individual methods showed variation anomalies of up to  $\pm 60$  days. Cong et al. (2012) demonstrated that across five different methods about 24% of temperate China showed a standard deviation for GUD larger than one month. However, which method performs better in terms of specific vegetation types remains unknown because of a lack of necessary and rigorous validation (Shen et al., 2015; Liu et al., 2017). Recently, numerous studies have indicated that Zhang's logistic method is increasingly considered a suitable choice in regional and global phenology research (Zhang et al., 2003; Zhu et al., 2012; Shen et al., 2014; He et al., 2018b). Nevertheless, some studies have argued that the cumulative logistic method may be more appropriate because it can overcome the misinterpretation of non-ideal S-shaped vegetation growth (Hou et al., 2014; Wu et al., 2016). However, these methods have yielded inconsistent results in GUD estimation accuracy in different studies (Wu et al., 2016; Liu et al., 2017). Thus, a comprehensive comparison of different methods in GUD extraction is of importance to accurately quantify the response of vegetation phenology.

Therefore, the primary objectives of this study were to: (1) present a comprehensive assessment of different GUD extraction algorithms for winter wheat based on 8-day EVI data, as well as ground observed GUD in the North China Plain (NCP); (2) quantify the combined effect of hydrothermal variation on winter wheat GUD by considering the non-identical lag time response of GUD to hydrothermal variables; (3) investigate the interactions between winter wheat GUD and GPP. The results may aid in diagnosing the responses of vegetation phenology to regional climate factors and further understanding in the linkage between vegetation structure and function.

## 2. Materials and methods

### 2.1. Study area

The NCP in this study includes the municipalities of Beijing and Tianjin, and provinces of Shandong, Hebei, Shanxi, Henan, Anhui and Jiangsu, which is highly consistent with that of Liu et al. (2017) (Fig. 1). The climate of this region is a typical temperate monsoon climate, characterized by a hot and rainy summer and a cold and dry winter, with the mean annual average air temperature and mean annual precipitation decreasing from southeast to northwest. The NCP is one of the major winter wheat production bases in China, dominated by a typical double cropping system of rotational winter wheat and summer maize cultivation (Tao et al., 2015). Winter wheat in this area is sown in late September to early October and harvested between late June and early July of the following year, with the total life cycle of 230 to 260 days.

### 2.2. Datasets

The enhanced vegetation index (EVI) is less affected by soil background and atmospheric noise, while remains sensitive to change in high canopy region where the normalized difference vegetation index (NDVI) easily becomes saturated (Huete et al., 2002; Xiao et al., 2003). In this study, we used EVI instead of the more widely used NDVI to

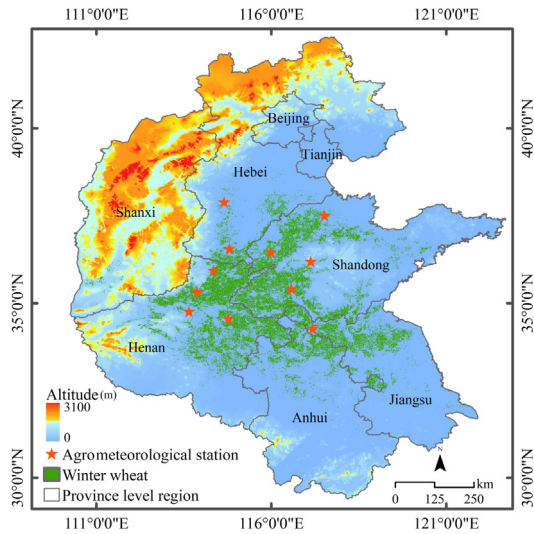


**Fig. 1.** Location of the North China Plain and spatial distribution of the 11 agrometeorological stations.

infer GUD for winter wheat. EVI dataset was obtained from the Center for Spatial Analysis, University of Oklahoma, calculated from 8-day MOD09A1 reflectance data (Zhang et al., 2017). In this dataset, missing observations and low-quality data (affected by atmospheric conditions such as clouds and aerosols) were rigorously addressed based on the MOD09A1 quality assurance layer and the Best Index Slope Extraction algorithm, and gaps were filled by linear interpolation and smoothed using a Savitzky-Golay filter (Zhang et al., 2017; Chang et al., 2019). This dataset, which has spatial resolution of 500 m and temporal resolution of 8-day from 2000 to 2015, could provide more temporal information depicting winter wheat growth.

The GPP product was the latest generation of the MOD17A2H GPP product version 6 (<https://lpdaac.usgs.gov/products/mod17a2hv006>), a cumulative 8-day composite of values with 500 m spatial resolution, produced after significant revisions of the calibration approach relative to previous versions (Lyapustin et al., 2014; Chen et al., 2019). Although some potential uncertainties from various inputs still exist (Zhu et al., 2016; Wang et al., 2017a; Wang et al., 2019), MOD17A2H GPP has been demonstrated to agree relatively well with annual GPP derived from flux towers in China (Zhu et al., 2016; Wang et al., 2019), and to be most effective at estimating the dynamics of GPP at some cropland sites in the NCP (Zhu et al., 2016) and other places (Wang et al., 2017a). It has also been used widely in global and regional carbon cycle estimations.

To analyze the relationships between hydrothermal variation and winter wheat GUD, spatial meteorological data including monthly mean maximum air temperature ( $T_{max}$ ), mean minimum air temperature ( $T_{min}$ ) and total precipitation (TP) data from 2001 to 2015 with a resolution of  $1 \times 1$  km, were generated from 604 meteorological stations across China using AUSPLINE software (Guo et al., 2019). The EVI and GPP data were resampled at a spatial resolution of  $1 \times 1$  km using ArcGIS software, in accordance with the monthly meteorological data.

Land use maps for two periods (2000 and 2015) with a spatial resolution of  $1 \times 1$  km, and were obtained from the Resources and Environment Data Center, Chinese Academy of Sciences (<http://www.igsnr.cas.cn>). First, land use maps were resampled for consistent resolution with the monthly meteorological data using ArcGIS software. We then used the cropland map for 2015 to mask the cropland map for 2000 and removed any changes in cropland. After that, we applied a sixth-order polynomial function to smooth the EVI time series for the remaining cropland, and winter wheat cultivation zones with a spatial resolution of  $1 \times 1$  km were identified, mainly by applying the second-order difference method for each year from 2001 to 2015. Only the successive

winter wheat plantation region during 2001–2015 was used for further analysis (Guo et al., 2019).

The winter wheat GUD observation data for the period of 2001–2009, recorded at the national agrometeorological stations, was collected from the Chinese Meteorological Administration (CMA). To obtain valid observation GUD from these raw records, we performed the following criteria: (1) stations with winter wheat GUD records before early January or after May were excluded because it is impossible that winter wheat greens up in the NCP (Guo et al., 2016; Wang et al., 2017b); (2) stations located far from the winter wheat cultivation area were dropped. Accordingly, a total of ninety nine winter wheat GUD records from 11 agrometeorological stations were selected (Fig. 1).

### 2.3. Determination of GUD

In this study, four methods were employed to determine winter wheat GUD: RCCmax, Kmax, CRmax, and cumCRmax. First, we attempted to eliminate any residual contamination in winter wheat EVI arising from summer crop EVI in the double cropping system by defining the minimum EVI occurrence time of May to early July as the end of winter wheat growth for each pixel. Secondly, to remove the disturbances (e.g., drought, snow) in EVI during the winter and spring seasons as much as possible, the minimum EVI value before the maximum EVI value during the winter wheat growth period was identified to replace the original EVI values prior to it. After that, we determined winter wheat GUD by using the following algorithms.

#### 2.3.1. RCCmax

In this method, GUD was determined as the inflection point of a logistic fitted curve of EVI using the method of Zhang et al. (2003). Specifically, a four-parameter logistic function was first used to fit the 8-day interval EVI data from the start of a year to the time of maximum EVI during the winter wheat growth period. Then, GUD was defined as the day when the rate of change in curvature (RCC) reached its first local maximum value (Liu et al., 2017; Shen et al., 2014), as follows:

$$EVI_t = \frac{c}{1 + e^{a+bt}} + d \quad (1)$$

$$RCC = b^3 cz \left\{ \frac{3z(1-z)(1+z)^3 [2(1+z)^3 + b^2 c^2 z]}{[(1-z)^4 + bcz^2]^{2.5}} \right\} - \frac{(1+z)^2 (1+2z-5z^2)}{[(1+z)^4 + (bcz^2)]^{1.5}} \quad (2)$$

where  $t$  represents day of year,  $EVI_t$  is the EVI value at time  $t$ ,  $a$  and  $b$  are fitting parameters, the sum  $c$  and  $d$  is the maximum EVI,  $d$  is the minimum EVI,  $z = e^{(a+bt)}$ , and  $T$  represents day of year at the daily scale.

#### 2.3.2. Kmax

GUD in this case was calculated as follows (Guo et al., 2019; Hou et al., 2014). First, we fitted a four-parameter logistic function to the cumulative EVI ( $cumEVI$ ) for the entire winter wheat growth period. Additionally, GUD was defined as the day when the curvature ( $K$ ) of the fitted four-parameter logistic  $cumEVI$  curve reached its maximum (Eq. (4)):

$$cumEVI_t = \sum_{i=1}^t EVI_i \quad (3)$$

$$K = -\frac{BCZ(1-Z)(1+Z)^3}{[(1+Z)^4 + (BCZ)^2]^{3/2}} \quad (4)$$

where  $t$  represents the day of year,  $cumEVI_t$  is the cumulative EVI from the start to time  $t$  at 8-day temporal interval,  $A$  and  $B$  are fitting parameters of the four-parameter logistic function fitted  $cumEVI$ , the sum  $C$

and  $D$  is the maximum cumEVI,  $D$  is the minimum cumEVI,  $Z = e^{(A+BT)}$ , and  $T$  represents day of year at the daily scale.

### 2.3.3. CRmax and cumCRmax

In these methods, GUD was extracted based on the maximum change rate (CR) of the fitted daily EVI (Shen et al., 2014). However, unlike previous studies (Cong et al., 2012; Jeong et al., 2011), we determined GUD as the day when the change rate of the four-parameter logistic function-fitted EVI (CRmax) and the four-parameter logistic function-fitted cumEVI (cumCRmax) reached their direct maximum, following Liu et al. (2017):

$$CR = \frac{EVI_{T+1} - EVI_T}{EVI_T} \quad (5)$$

where  $EVI_T$  (cumEVI<sub>T</sub>) represents the four-parameter logistic function-fitted daily EVI (cumEVI) at day  $T$  of the year.

### 2.4. Statistical analysis

Considering some extreme variation in GUD due to abrupt EVI curves, we first identified the extreme outliers of the derived GUD using the interquartile range method (IQR) for each method (Barbato et al., 2011); these were defined as any value greater than  $Q3 + 3 \times IQR$  or less than  $Q1 - 3 \times IQR$  of the time series GUD for each pixel during 2001–2015. Then, the extreme outliers of GUD and the corresponding climate variables from 2001 to 2015 were removed in the next analysis. We used the determination coefficient ( $R^2$ ), root mean square error (RMSE), and difference between estimations and observations (Bias) to evaluate the performance of GUD extraction (mean GUD from  $17 \times 17$  pixels near the center of each ground station for each year) with winter wheat GUD observations data. To explain the effects of hydrothermal variations on GUD, we developed a multiple linear regression model between  $\Delta GUD$  and pre-season  $\Delta T_{min}$ ,  $\Delta T_{max}$ , and  $\Delta TP$  at regional and pixel scales. Here,  $\Delta$  means the first-difference time series (i.e., the difference in values from the following year to the current year)

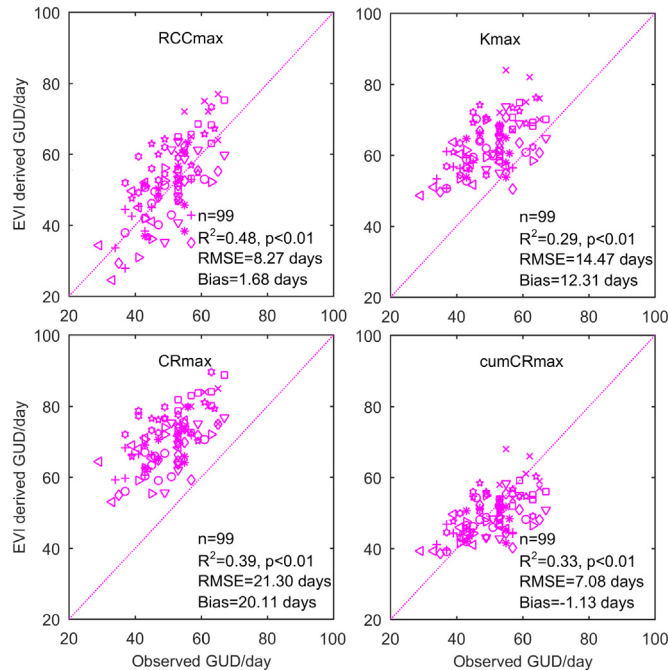


**Fig. 2.** Validation of annual GUD derived from the different methods in relation to the observed GUD for the 11 agrometeorological stations. The various red symbols represent the 11 agrometeorological stations. The red dashed line is the 1:1 relationship.

of GUD and climate variables ( $T_{min}$ ,  $T_{max}$ ,  $TP$ ), which was used to eliminate the non-climatic influences on GUD, such as human activity (Lobell and Field, 2007; Zhang et al., 2016b). Furthermore, the pre-season was determined for  $T_{min}$  as the period preceding multiyear averaged GUD during 2001–2015 in which  $\Delta T_{min}$  had the largest partial correlation coefficient (absolute value) with  $\Delta GUD$ , with the pre-season  $\Delta T_{max}$  and  $\Delta TP$  set as control variables. In other words, we calculated the partial correlation coefficients between  $\Delta GUD$  and  $\Delta T_{min}$  for previous months (ranging from 0 to 3) before the multiyear average GUD, at 1-month intervals. The candidate previous month with the largest absolute partial correlation coefficient was finally selected as the pre-season. The pre-seasons of  $\Delta T_{max}$  and  $\Delta TP$  on  $\Delta GUD$  were assessed in a similar way. The slope of the linear regression of GPP against year from 2001 to 2015 was determined as the temporal trend in GPP. To further understand the interannual variation in winter wheat GPP, we compared its temporal trend for the whole GPP over the lifetime of winter wheat ( $GPP_w$ ) and the cumulative GPP after GUD ( $GPP_{GUD}$ ). Furthermore, correlation coefficients between  $\Delta GUD$  and  $\Delta GPP_w$  ( $GPP_{GUD}$ ) were calculated to identify the impact of GUD on GPP, and we also determined a correlation coefficient between  $\Delta GPP_w$  ( $GPP_{GUD}$ ) of the previous year and  $\Delta GUD$  to quantify the feedback of GPP on GUD. It should be noted that the extreme outliers of GUD and the corresponding GPP from 2001 to 2015 were also removed in this correlation analysis. All of the statistical analyses were performed at a significance level of 0.10.

## 3. Results

### 3.1. The performance of satellite-derived GUD

As illustrated in Fig. 2, all methods captured the observed winter wheat GUD across the 11 agrometeorological stations during 2001–2009, varying in their predictive strength. In general, GUD based on the Kmax and CRmax algorithms was obviously overestimated when compared with that from the RCCmax and cumCRmax methods. This was especially true for the CRmax algorithm. GUD predicted from the cumCRmax algorithm showed the lowest RMSE (7.08 days), Bias (−1.13 days) and  $R^2$  (0.33), which means that the model could explain only 33% of the observed GUD. By contrast, GUD based on the RCCmax method presented a better correlation with the observed GUD ( $R^2 = 0.47$ ,  $p < 0.01$ ), but with a little larger RMSE (8.27 days) and Bias (1.68 days). Additionally, Fig. 3 showed that mean GUD derived from the RCCmax algorithm showed good performance in capturing the interannual variation and spatial pattern of the mean observed GUD over the agrometeorological stations, with both  $R^2$  values  $>0.60$ , whereas mean GUD calculated from the cumCRmax algorithm did not match well with the interannual variation of mean observed GUD ( $R^2 = 0.26$ ). Moreover, strong relationships between GUD from the RCCmax algorithm and the observed GUD were found for all stations except Liaocheng. We then use GUD derived from the RCCmax algorithm for subsequent analysis.

### 3.2. Effect of hydrothermal variation on the spatiotemporal variation in GUD

The regression model demonstrated good performance in explaining the interannual GUD variation over the NCP (Fig. 4). The GUD for 82.05% of the total pixels could be significantly explained by the three climatic factors, and the explanation ability ranged up to 96.93% for some regions. In particular, the explanation ability in the ranges of 40–60%, 60–80% and  $>80\%$  accounted for about 26.43%, 42.44%, and 13.18% of the total pixels, respectively (Fig. 4b). Additionally, the explanation area was approximately 36.78% greater than that without considering the time lag effect of hydrothermal variation (Fig. S1a), and about 1.37% larger than the explanation area when the time lag effects were considered, but the remarkable differences in lag time of hydrothermal factors were ignored (Fig. S1b).

### 3.3. Interaction effects between GUD and plant productivity

The multi-year mean  $GPP_W$  generally exhibited an increasing trend from the north area to the south area, i.e., from  $\leq 300 \text{ g C m}^{-2} \text{ yr}^{-1}$  in the contiguous area of Hebei and Shandong provinces to  $500 \text{ g C m}^{-2} \text{ yr}^{-1}$  in the southern region of Jiangsu and Anhui provinces, with a regional average of about  $406.06 \text{ g C m}^{-2} \text{ yr}^{-1}$  (Fig. 5a). Furthermore, the proportion of  $GPP_{GUD}$  also showed a large spatial variation. For example, in the central region of the NCP, the  $GPP_{GUD}$  accounted for  $>85\%$  of the  $GPP_W$ , but it accounted for a relatively lower (about 80–85%) amount over most of the remaining area (Fig. 5b). For the whole study area,  $GPP_{GUD}$  accounted for approximately 84.54%.

Average  $GPP_W$  and  $GPP_{GUD}$  over the NCP revealed a significant ( $p < 0.10$ ) increase trend during the study period, with an increase

rate of 6.81 and  $4.05 \text{ g C m}^{-2} \text{ yr}^{-2}$ , respectively (Fig. 6). Spatially,  $GPP_W$  in about 70% of all pixels increased significantly, distributed mostly in the central and northern parts of the area. Only about 1.94% of all pixels showed significant decreases in  $GPP_W$ , scattered mainly in the western and eastern parts of the NCP (Fig. 7a). In comparison, the significant increase in  $GUD_{GUD}$  pixels (54.26%) located in the northeastern and southeastern parts of the NCP, was approximately 0.6 times that for  $GPP_W$ . Areas with decreased  $GPP_{GUD}$  were up to 14.36% of all pixels, with 3.68% of all pixels showing significant changes (Fig. 7b).

The regional averaged GUD over the NCP was slightly negatively related with  $GPP_W$  ( $p = 0.36$ ) and  $GPP_{GUD}$  ( $p = 0.12$ ). Spatially, widespread negative correlations between GUD and  $GPP_W$  across the NCP were observed for 75.31% of the total pixels, with significantly negative correlations characterizing 24.76% of all pixels (Fig. 8a). Compared with  $GPP_W$ , the impact of GUD on  $GPP_{GUD}$  was much stronger (Fig. 8b). GUD was negatively related with  $GPP_{GUD}$  over about 88.44% of all pixels, with significantly negative relationship in 35.73% of all pixels, located mainly in the northern and central areas of the NCP, which indicates that the advance in GUD could strongly boost winter wheat GPP after green up.

The GUD averaged over the NCP was significantly positively correlated with previous-year  $GPP_W$  and  $GPP_{GUD}$ , with correlation coefficients of about 0.56 ( $p < 0.05$ ) and 0.58 ( $p < 0.05$ ), respectively. Furthermore, as exhibited in Fig. 9, GUD from 83.17% of the pixels was positively related with previous-year  $GPP_{GUD}$ , with about 26% of all pixels showing significant relationships (Fig. 9b); these were mainly located in the northwestern and central-south areas of the NCP. In contrast to  $GPP_{GUD}$ , the correlation between GUD and previous-year  $GPP_W$  appeared to have a similar spatial pattern. Significantly positive correlations between GUD and previous-year  $GPP_W$  were observed in  $>28.01\%$  of all pixels. The correlation was especially stronger in most parts of the northwestern and central areas, but it was weaker or even reversed in some southern parts (Fig. 9a). This suggests that the previous year's total GPP during the whole winter wheat growing time is probably critical to GUD variation in the NCP.

To analyze the relationship between GUD and previous-year  $GPP_W$  further, we calculated correlation coefficients between GUD and previous-year  $GPP_W$  along the spatial gradient of long-term average  $GPP_W$  (Fig. 10). The correlation between GUD and previous-year  $GPP_W$  increased with increases in  $GPP_W$  below  $350\text{--}400 \text{ g C m}^{-2} \text{ yr}^{-1}$ , and then decreased. That is, the relationship between GUD and previous-year  $GPP_W$  weakened when  $GPP_W$  fell below or exceeded  $350\text{--}400 \text{ g C m}^{-2} \text{ yr}^{-1}$ , implying that winter wheat GUD is most sensitive to previous-year  $GPP_W$  when  $GPP_W$  is about  $350\text{--}400 \text{ g C m}^{-2} \text{ yr}^{-1}$ .

## 4. Discussion

### 4.1. Comparison of different methods in GUD identification

Accurately extracting crop spring phenology has been considered to be of profound significance to our understanding of responses of vegetation phenology to climate change and crop production (Cong et al., 2012; Liu et al., 2018b). The cumulative vegetation index (CVI) can effectively overcome the interference of environmental factors (Hou et al., 2014), and GUD extraction based on CVI has been shown to perform better (Wu et al., 2016; Wang et al., 2017b). However, compared with the observed 99 GUD from the 11 agrometeorological stations, our result indicates the Kmax and cumCRmax method performed a smaller  $R^2$  among the four algorithms. The difference may be caused by two possible reasons. The first reason might be that natural vegetation focused by the previous studies is usually controlled by environmental stresses (e.g., droughts, diseases) and often follows a non-ideal S-shaped temporal profile (Cao et al., 2015), whereas agricultural managements make winter wheat growth different from natural ecosystems (Fang et al., 2018). In addition, to make a well-defined S-shaped logistic temporal profile, we removed the possible winter-spring disturbances in EVI by using the minimum EVI value before the maximum EVI

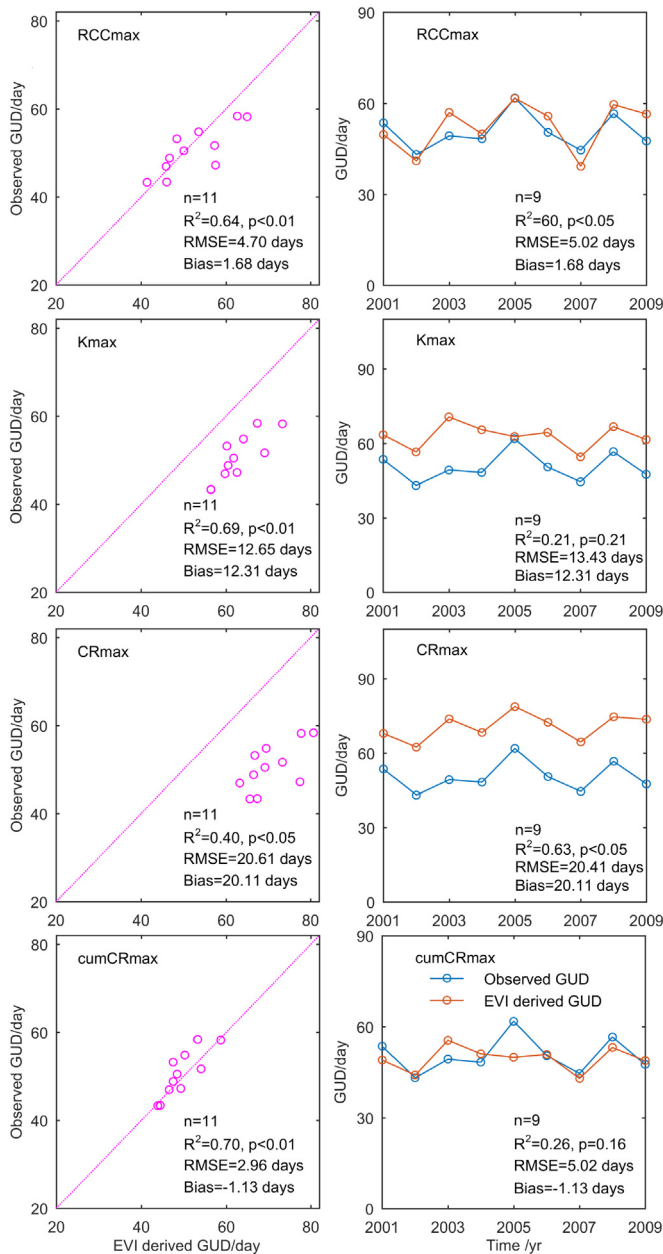


**Fig. 3.** Spatial relationship between multi-year mean GUD derived from the different methods and the observed GUD (the left column) and interannual trends of regional mean GUD derived from the different methods and the observed GUD (the right column) for the 11 agrometeorological stations. The red dashed line is the 1:1 relationship.

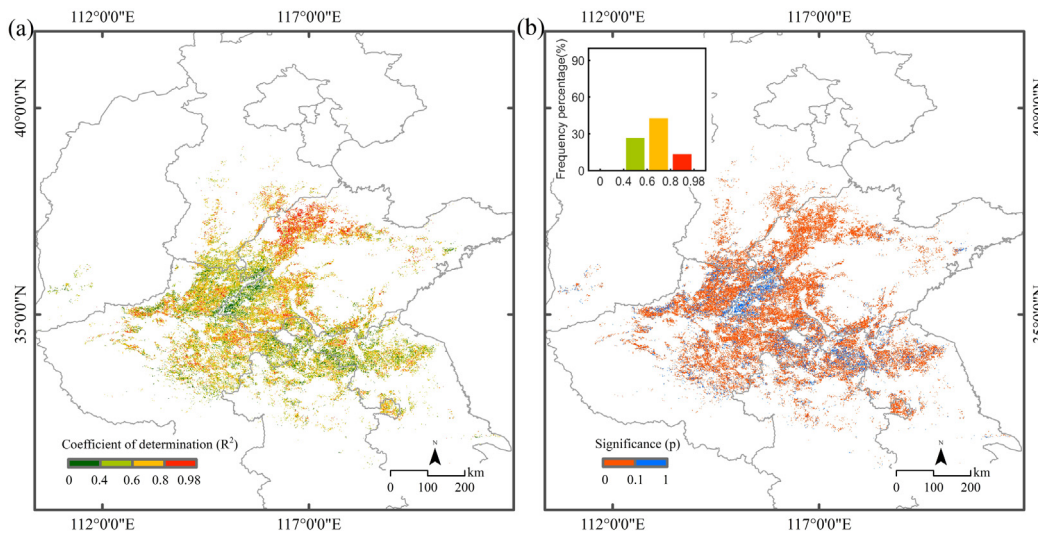


**Fig. 4.** Spatial distribution of the determination coefficient ( $R^2$ ) of the multiple linear regression model between GUD and the pre-season climatic factors by considering the non-identical lag time effects of climate variables for the period 2001–2015 (a) and the levels of significance (b). The inset at the upper-left in (b) shows the frequency distribution of the determination coefficient corresponding to the significant pixels indicated by the map legend in (a).

value to replace the original values before this minimum (Guo et al., 2019). This result provides strong evidence that the merits of a specific method are dependent on the types of ecosystem. Meanwhile, we found that the cumCRmax method did best in estimating the spatial pattern of winter wheat GUD ( $R^2 = 0.70$ , RMSE = 2.96, and Bias =  $-1.13$ ), but was not a good method to capture the interannual variation of winter wheat GUD. This is probably related with the cumulative EVI curve. First, GUD estimated from the cumCRmax method was usually earlier than those with other methods, and relatively close to the average observed GUD. Second, the cumulative EVI generally had a spatial pattern from south toward north in the NCP due to the unique hydrothermal condition. In addition, the cumCRmax method may be problematic in identifying GUD which should occur at later time since the change rate tended to be smaller because of the larger cumulative EVI value at later time.

Our result found that GUD derived from the RCCmax algorithm not only captured the spatial distribution of winter wheat GUD, but also matched well with its interannual variation. Moreover, GUD derived from the RCCmax algorithm showed a stronger correlation with

observations compared with the previous study (Liu et al., 2017). This improvement may mainly be caused by the finer temporal resolution of EVI data and the well-defined S-shaped logistic temporal profile constructed by the data preprocessing (Guo et al., 2019). On one hand, satellite temporal resolution plays an important role in the GUD estimations (Liu et al., 2017), the more points available in the time series, the more accurate information of vegetation growth (Ahl et al., 2006). On the other hand, the effectiveness of the RCCmax algorithm is hugely dependent on the S-shaped temporal profile of vegetation indices (Cao et al., 2015). These findings indicate that the RCCmax algorithm based on 8 day MODIS EVI is suitable for the analysis of spatial and temporal variations in winter wheat GUD over the NCP. However, it should be noted that the RCCmax algorithm slightly overestimated the observed winter wheat GUD. The discrepancy can be expected because of the different definition of GUD and the classical point vs. pixel comparison errors in remote sensing assessments (White et al., 2009), which highlights the ground observation network with an explicit purpose of satellite GUD assessment should be established to improve the satellite estimation.

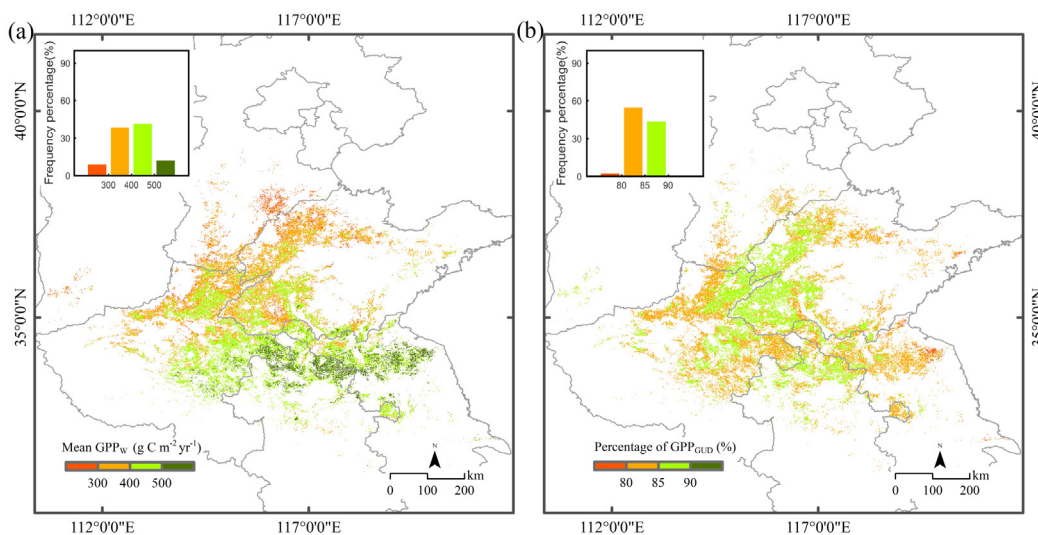


**Fig. 5.** Spatial distribution of the mean  $GPP_w$  (a) and the percentage of  $GPP_{GUD}$  (b) over the NCP during 2001–2015. The inset at upper-left in (a) indicates the frequency distribution of mean  $GPP_w$ . The inset in upper-left in (b) denotes the frequency distribution of the  $GPP_{GUD}$  proportion corresponding to values indicated by the map legend.

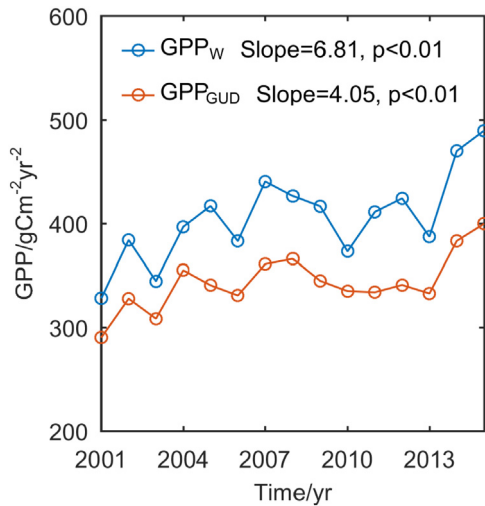


**Fig. 6.** Interannual variation in GPP over the NCP during 2001–2015.

Additionally, in areas with missing ground measurements, an ensemble approach using multiple methods has been suggested to be more powerful for GUD estimation than using single method alone (Shen et al., 2015; Wang et al., 2015), because satellite-derived GUD differs dramatically among different methods (Cong et al., 2012; Shen et al., 2014). Interestingly, our results showed GUD inferred from the cumCRmax method presented a significant correlation with that from the Kmax algorithm ( $R^2 = 0.98$ ), and GUD based on the RCCmax algorithm significantly correlated with that from the CRmax algorithm ( $R^2 = 0.87$ ) over the 11 agrometeorological stations from 2001 to 2009 (Fig. S2). This argues that when an ensemble approach in the spring vegetation green-up onset estimation is performed, reconstructing distinct satellite derived vegetation curve is extremely necessary.

**4.2. Contributions of GUD to GPP variation**

Generally agreeing with the mean of nine TRENDY models (Yao et al., 2018), we found that the winter wheat GPP showed a descending gradient from south to north. This can be attributed to the colder climate and shorter growing season in the northern region. The climate of the southern region is relatively humid, with good thermal conditions

appropriate for vegetation growth. In addition, our analyses found a strong and extensive increasing trend for annual winter wheat GPP over the NCP during 2001–2015, with almost 70% of all pixels experiencing a significant increase. This is generally consistent with the results of previous studies (Ichii et al., 2017; Mo et al., 2018; Yao et al., 2018). However, large uncertainties in the corresponding magnitude existed between our results and those of previous studies, which could be related to the differences in GPP calculation model structure and parameterization (Zhu et al., 2014; Sitch et al., 2015), the period of investigation (Piao et al., 2007), or the precision of input data (Wang et al., 2017a). Moreover, it probably resulted from the typical rotational winter wheat and summer maize cultivation method, within which only winter wheat was the focus in our study.

Numerous studies have documented that GPP can be considerably enhanced by the prolonged vegetation growing season induced by climatic factors (Piao et al., 2007; Richardson et al., 2010; Xia et al., 2015). For instance, Zhou et al. (2016) found that the starting date of the growing season was related strongly to annual GPP increase, with a correlation coefficient of about  $0.72 \pm 0.20$ . Variation in growing season onset could account for approximately  $13.8 \pm 13.70\%$  of annual GPP in some regions (Zhou et al., 2017). Similarly, our result showed that GUD variation was strongly and negatively related to winter wheat gross primary production after greening up, accounting for 88.44% of the total pixels (significant for 35.73% of the total pixels). The following reasons may be responsible for this finding. First, advanced GUD may potentially lead to larger display of leaf area, thereby enhancing canopy interception of solar radiation (Luysaert et al., 2007; Richardson et al., 2009). The increase in GPP could be also related to the photosynthetic capacity of single leaves in the leaf expansion period. It has been suggested that leaf photosynthetic capacity exhibits a dramatic increase from spring to early summer, exerting a remarkable influence on GPP (Muraoka et al., 2010). In addition, an alternative explanation is that, earlier GUD usually associates with higher temperatures, which may stimulate microbial activity and accelerate nitrogen mineralization, then enhance photosynthesis for the remainder of the growing season (Richardson et al., 2010). In addition, we found a weak positive correlations between GUD and total GPP during the whole life cycle in some southern parts of the NCP, which could be related to increased winter wheat growth during the overwinter time due to climate warming, suggesting that more attention should

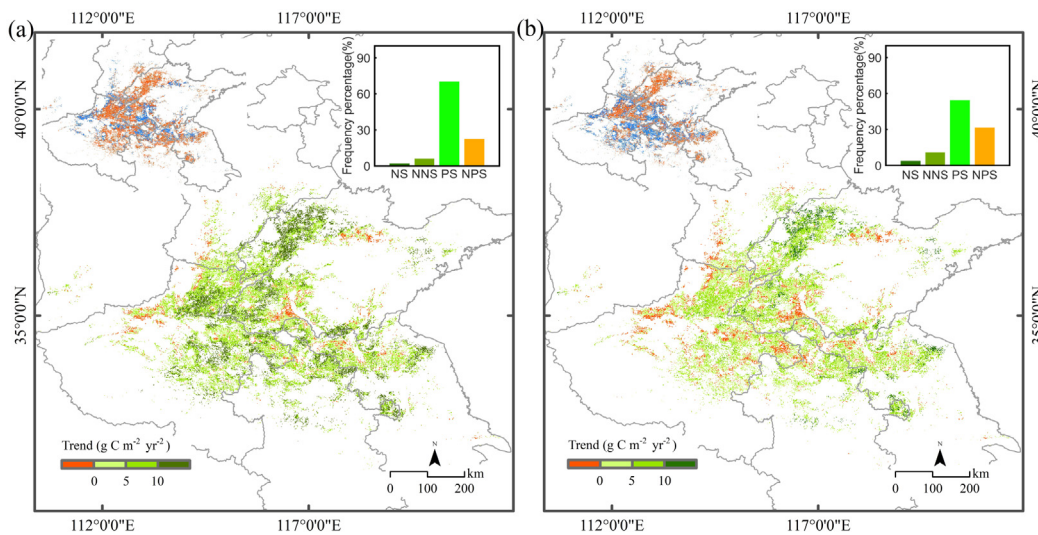


**Fig. 7.** Spatial pattern of the temporal trends in mean  $GPP_W$  (a) and  $GPP_{GUD}$  (b) from 2001 to 2015. The inset at upper-left indicates pixels significant at  $p < 0.10$  (red), and non-significant pixels (blue). The inset at upper-right shows the corresponding frequency level of significance. NS, NNS, PS and NPS indicate significantly negative, not significantly negative, significantly positive, not significantly positive changes, respectively.

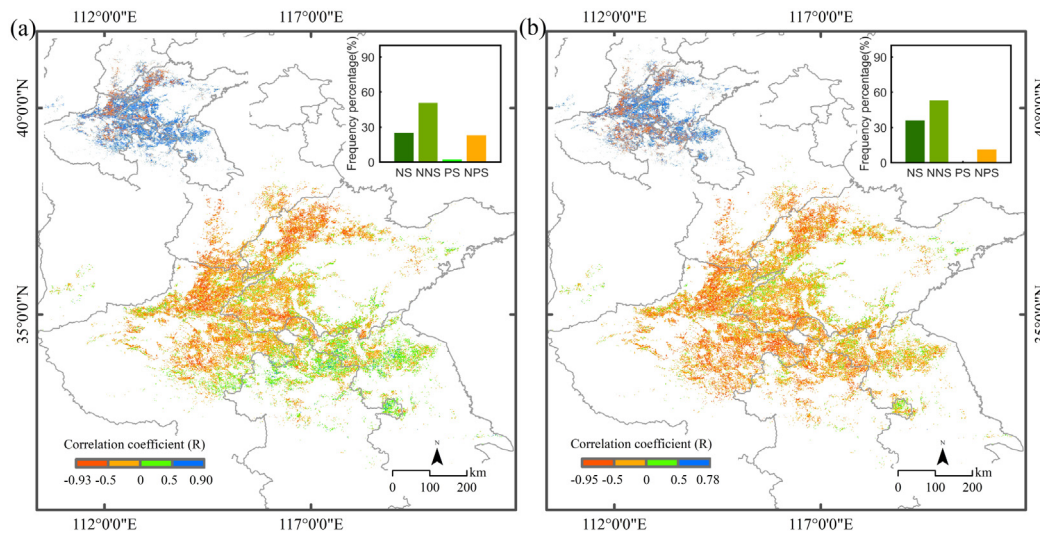


**Fig. 8.** Spatial pattern of the interannual correlations of GUD with GPP<sub>w</sub> (a), and GPP<sub>GUD</sub> (b). Insets at upper-left indicate pixels significant at  $p < 0.10$  (red), and those with non-significant relations (blue). Insets at upper-right show the corresponding frequency. NS, NNS, PS, and NPS indicate significantly negative, not significantly negative, significantly positive, not significantly positive relationships, respectively.

be given to the precise response of GPP to climatic factors for the overwinter crop.

#### 4.3. Role of hydrothermal variation and GPP on GUD

Recently, an increasing number of studies have indicated that the responses of GUD to climate have a certain time lag (Cong et al., 2013; Shen et al., 2014; Wang et al., 2017b; Guo et al., 2019). In general, GUD has been shown to be most significantly related to the pre-season temperature and total precipitation at 2–3 months before the mean GUD (Cong et al., 2013), but it exhibits a strong site and climatic parameter dependence (Liu et al., 2017). In our study, when time lag impacts were considered, the three climatic factors explained GUD variation for 82.05% of all pixels; this area could be about 1.37% larger than that when considering only the identical lag time of different climate factors and approximately 36.78% higher than when ignoring the time lag effect altogether. This result confirmed the significant role of the time lag effect

of climate factors in influencing GUD variation, providing us with important information for understanding climate-vegetation interaction, and it also indicated that other factors may also play important roles in GUD. Previous studies have suggested the spring growth initiation of plants could be related to other biological and environmental factors, such as photoperiod (Zohner et al., 2016), chilling requirement (Fu et al., 2015; Cong et al., 2017), and nutrient availability (Estiarte and Penuelas, 2015). Further experimental studies are therefore needed to explore the physiological mechanisms underlying the impacts of these factors on winter wheat green up date.

Additionally, our result indicated that GUD over the NCP was positively correlated with previous-year GPP<sub>w</sub> and GPP<sub>GUD</sub> for >80% of all pixels, especially with GPP<sub>w</sub>, suggesting that previous-year GPP during the whole life cycle is probably critical to GUD variation in the NCP. One possible reason for this finding is that higher GPP in the previous year resulted in increased biomass, which subsequently provided greater organic matter input and thereby enhanced vegetation growth in next

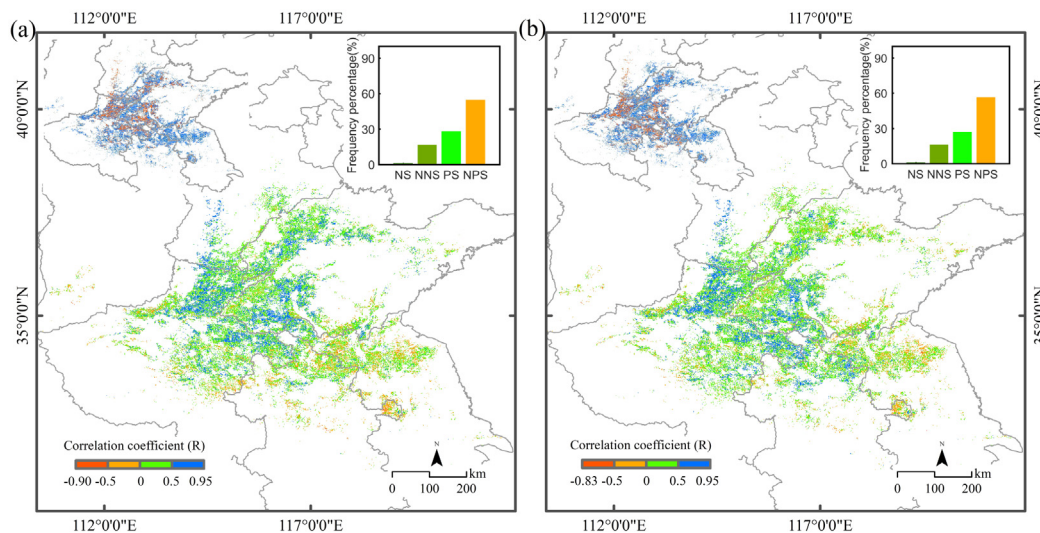


**Fig. 9.** Spatial pattern of the interannual correlations between GUD and previous-year GPP<sub>w</sub> (a) and GPP<sub>GUD</sub> (b). Insets at upper-left indicate pixels with significant at  $p < 0.10$  (red), and those that were not significant (blue). Insets at upper-right show the corresponding frequency. NS, NNS, PS, and NPS indicate significantly negative, not significantly negative, significantly positive, not significantly positive relationships, respectively.

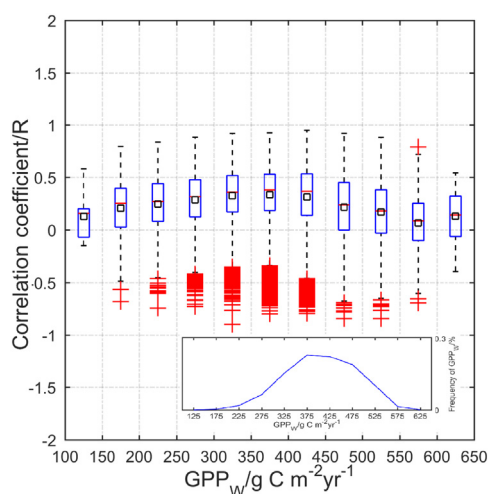


**Fig. 10.** Variation in correlation coefficient between GUD and previous-year  $GPP_w$  along the spatial gradient of long-term average  $GPP_w$ . The bottom and top edges of each blue box indicate the 25th and 75th percentiles, respectively. The horizontal red line in each blue box represents the median value. The black square in each blue box represents the mean value. The black whiskers extend to 1.5 times the interquartile range. Red crosses indicate outliers. The inset at the right bottom shows the frequency distributions of corresponding long-term average  $GPP_w$ .

year. As is known, winter wheat-summer maize cropping is one of the most popular cropping systems in the NCP. In this system, winter wheat straw is often returned to the soil by residue and no-tillage management (Zhao et al., 2015; Zhang et al., 2016a, 2016b; Zhang et al., 2018), which could effectively alter concentrations of soil organic matter and soil nitrogen (Zhang et al., 2016a, 2016b), soil aggregate structure (Zhang et al., 2018), and microbial community (Hu et al., 2018), effectively improving soil fertility and vegetation growth (Zhao et al., 2019). In addition, our results showed that GUD was most sensitive to GPP when the whole GPP was about 350–400  $g\ C\ m^{-2}\ yr^{-1}$ . This pattern could be explained by the effect of soil organic matter derived from GPP. For example, the lower GPP is, the lower the organic matter content will be (Yang et al., 2017); the lower decomposition rate (Piao et al., 2008) in the cold northern parts of the NCP resulted in only slight increases in soil fertility, which had a limited effect on vegetation growth. However, as GPP increases, greater organic matter content and decomposed organic matter potentially lead to a greater effect on GUD. Above the aforementioned threshold, the relationship between GPP and GUD weakened, probably due to interactions between soil organic carbon and other environment factors. For instance, Oldfield et al. (2019) found that increases in crop yields with higher concentrations of soil organic carbon could level off at a certain threshold, and highlighted the interaction between soil organic carbon and nitrogen inputs in agricultural systems.

#### 4.4. The chain relationship among hydrothermal variation, GUD and GPP

As a critical link between climate change and vegetation productivity, changes in GUD and its impacts have been a major scientific issue of general concern to the scientific community (Xia and Wan, 2013; Piao et al., 2015; Xia et al., 2019). So far, a great number of studies have reported the spatiotemporal variation of GUD and its responses to hydrothermal changes at various scales (Jeong et al., 2011; Shen et al., 2015). Several other studies suggested that climate induced shifts in GUD may considerably influence ecosystem functions. However, the knowledge of the chain relationship of climate change, phenological processes, and ecosystem functions is relatively weak. Based on a comprehensive assessment of the ability of GUD extraction methods, our analyses not only reduced uncertainty in estimating GUD for winter wheat in the NCP, but also provided innovative insights in the chain reaction

among hydrothermal variation, GUD and GPP. We found that precipitation and temperature jointly determined the GUD variation for >82.05% of the winter wheat area in the NCP, with an average explanation ( $R^2$ ) of 66.84%. Furthermore, climate induced changes in GUD presented a negatively linear relation with  $GPP_{GUD}$  in 88.44% of the winter wheat area (with a mean explanation ( $R^2$ ) of 19.77%), significantly in 35.75% of the total pixels with a mean slope of  $1.89\ g\ C\ m^{-2}\ yr^{-1}\ day^{-1}$ . At the last link of the chain, GPP in previous year had positive feedback effects on GUD for about 82.42% of the total pixels, and approximately 28.01% of the total pixels showed significantly positive feedback effects (mean linear slope of 0.15), suggesting that  $1\ g\ C\ m^{-2}\ yr^{-1}$  increase in previous-year GPP tends to advance GUD by 0.15 day. These findings indicate that sensitivity of GUD to changing climate could be amplified by the positive feedback effect from GPP variation, which is essential for better understanding the interactions between climate change and ecosystems.

## 5. Conclusion

Based on 8-day temporal resolution MODIS EVI data during 2001–2015, we found that GUD derived from the maximum curvature of the fitted four-parameter logistic cumulative EVI did not exhibit the desired performance for winter wheat in the NCP, whereas the RCCmax algorithm was more appropriate for monitoring spatiotemporal patterns of GUD variation. Consideration of the non-identical lag time effects of hydrothermal factors was very important for accurately revealing the response of GUD to hydrothermal variation. The advance of GUD could trigger winter wheat GPP after green up in northern and central areas of the NCP, but diminish total GPP over the whole winter wheat life cycle in some of the southern part of the NCP, suggesting that more attention should be given to the complex response of GPP to climate factors for the overwinter crop. In addition, previous-year GPP presented strong positive feedback effects to GUD variations for most parts of the NCP, characterized by a humped-shape pattern along the long-term average plant productivity. It provides useful information that can be used to improve our understanding of the interactions between ecosystem and climate change.

## Declaration of competing interest

The authors declare that they have no known competing financial interests or personal relationships that could have appeared to influence the work reported in this paper.

## Acknowledgments

This study was supported by the Natural Science Foundation of China (No. 41601580, 41671098, U1904210), Strategic Priority Research Program of the Chinese Academy of Sciences (No. XDA19040304), National Key Research and Development Program (No. 2017YFD0301106-1), Innovative Research Team of Henan Polytechnic University (No. T2018-4), Research Projects of Land and Resources in Henan Province (No. 20190450-7), and Open Foundation of Key Laboratory of Land Surface Pattern and Simulation, Chinese Academy of Sciences (No. LBKF201801).

## Appendix A. Supplementary data

Supplementary data to this article can be found online at <https://doi.org/10.1016/j.scitotenv.2020.138342>.

## References

- Ahl, D.E., Gower, S.T., Burrows, S.N., Shabanov, N.V., Myneni, R.B., Knyazikhin, Y., 2006. Monitoring spring canopy phenology of a deciduous broadleaf forest using MODIS. *Remote Sens. Environ.* 104 (1), 88–95. <https://doi.org/10.1016/j.rse.2006.05.003>.
- Badgley, G., Field, C.B., Berry, J.A., 2017. Canopy near-infrared reflectance and terrestrial photosynthesis. *Sci. Adv.* 3, e1602244. <https://doi.org/10.1126/sciadv.1602244>.

- Barbato, G., Barini, E.M., Genta, G., Levi, R., 2011. Features and performance of some outlier detection methods. *J. Appl. Stat.* 38 (10), 2133–2149. <https://doi.org/10.1080/02664763.2010.545119>.
- Cao, R., Chen, J., Shen, M., Tang, Y., 2015. An improved logistic method for detecting spring vegetation phenology in grasslands from MODIS EVI time-series data. *Agric. For. Meteorol.* 200, 9–20. <https://doi.org/10.1016/j.agrformet.2014.09.009>.
- Chang, Q., Xiao, X., Jiao, W., Wu, X., Doughty, R., Wang, J., Du, L., Zou, Z., Qin, Y., 2019. Assessing consistency of spring phenology of snow-covered forests as estimated by vegetation indices, gross primary production, and solar-induced chlorophyll fluorescence. *Agric. For. Meteorol.* 275, 305–316. <https://doi.org/10.1016/j.agrformet.2019.06.002>.
- Chen, Y., Gu, H., Wang, M., Gu, Q., Ding, Z., Ma, M., Liu, R., Tang, X., 2019. Contrasting performance of the remotely-derived GPP products over different climate zones across China. *Remote Sens.* 11 (16), 1855. <https://doi.org/10.3390/rs11161855>.
- Cong, N., Piao, S., Chen, A., Wang, X., Lin, X., Chen, S., Han, S., Zhou, G., Zhang, X., 2012. Spring vegetation green-up date in China inferred from SPOT NDVI data: a multiple model analysis. *Agric. For. Meteorol.* 165, 104–113. <https://doi.org/10.1016/j.agrformet.2012.06.009>.
- Cong, N., Wang, T., Nan, H., Ma, Y., Wang, X., Myneni, R.B., Piao, S., 2013. Changes in satellite-derived spring vegetation green-up date and its linkage to climate in China from 1982 to 2010: a multimethod analysis. *Glob. Chang. Biol.* 19 (3), 881–891. <https://doi.org/10.1111/gcb.12077>.
- Cong, N., Shen, M., Piao, S., Chen, X., An, S., Yang, W., Fu, Y.H., Meng, F., Wang, T., 2017. Little change in heat requirement for vegetation green-up on the Tibetan Plateau over the warming period of 1998–2012. *Agric. For. Meteorol.* 232, 650–658. <https://doi.org/10.1016/j.agrformet.2016.10.021>.
- Estiarte, M., Penuelas, J., 2015. Alteration of the phenology of leaf senescence and fall in winter deciduous species by climate change: effects on nutrient proficiency. *Glob. Chang. Biol.* 21 (3), 1005–1017. <https://doi.org/10.1111/gcb.12804>.
- Fang, Q., Zhang, X., Shao, L., Chen, S., Sun, H., 2018. Assessing the performance of different irrigation systems on winter wheat under limited water supply. *Agric. Water Manag.* 196, 133–143. <https://doi.org/10.1016/j.agwat.2017.11.005>.
- Fu, Y.H., Piao, S., Beeck, M.O.D., Nan, C., Zhao, H., Yuan, Z., Menzel, A., Janssens, I.A., 2014. Recent spring phenology shifts in Central Europe based on multi-scale observations. *Glob. Ecol. Biogeogr.* 23, 1255–1263. <https://doi.org/10.1111/gcb.12210>.
- Fu, Y.H., Zhao, H., Piao, S., Peaucelle, M., Peng, S., Zhou, G., Ciais, P., Huang, M., Menzel, A., Penuelas, J., et al., 2015. Declining global warming effects on the phenology of spring leaf unfolding. *Nature* 526, 104–107. <https://doi.org/10.1038/nature15402>.
- Ge, Q., Wang, H., Rutishauser, T., Dai, J., 2015. Phenological response to climate change in China: a meta-analysis. *Glob. Chang. Biol.* 21, 265–274. <https://doi.org/10.1111/gcb.12648>.
- Guo, L., An, N., Wang, K., 2016. Reconciling the discrepancy in ground- and satellite-observed trends in the spring phenology of winter wheat in China from 1993 to 2008. *J. Geophys. Res.-Atmos.* 121 (3), 1027–1042. <https://doi.org/10.1002/2015JD023969>.
- Guo, L., Gao, J., Hao, C., Zhang, L., Wu, S., Xiao, X., 2019. Winter wheat green-up date variation and its diverse response on the hydrothermal conditions over the North China Plain, using MODIS time-series data. *Remote Sens.* 11, 1593. <https://doi.org/10.3390/rs11131593>.
- Han, Q., Wang, T., Jiang, Y., Fischer, R., Li, C., 2018. Phenological variation decreased carbon uptake in European forests during 1999–2013. *For. Ecol. Manag.* 427, 45–51. <https://doi.org/10.1016/j.foreco.2018.05.062>.
- He, Y., Piao, S., Li, X., Chen, A., Qin, D., 2018a. Global patterns of vegetation carbon use efficiency and their climate drivers deduced from MODIS satellite data and process-based models. *Agric. For. Meteorol.* 256–257, 150–158. <https://doi.org/10.1016/j.agrformet.2018.03.009>.
- He, Z., Du, J., Chen, L., Zhu, X., Lin, P., Zhao, M., Fang, S., 2018b. Impacts of recent climate extremes on spring phenology in arid-mountain ecosystems in China. *Agric. For. Meteorol.* 260–261, 31–40. <https://doi.org/10.1016/j.agrformet.2018.05.022>.
- Hou, X., Gao, S., Niu, Z., Xu, Z., 2014. Extracting grassland vegetation phenology in North China based on cumulative SPOT-VEGETATION NDVI data. *Int. J. Remote Sens.* 35 (9), 3316–3330. <https://doi.org/10.1080/01431161.2014.903437>.
- Hu, N., Shi, H., Wang, B., Gu, Z., Zhu, L., 2018. Effects of different wheat straw returning modes on soil organic carbon sequestration in a rice-wheat rotation. *Can. J. Soil Sci.* 99 (1), 25–35. <https://doi.org/10.1139/cjss-2018-0094>.
- Huete, A., Didan, K., Miura, T., Rodriguez, E.P., Gao, X., Ferreira, L.G., 2002. Overview of the radiometric and biophysical performance of the MODIS vegetation indices. *Remote Sens. Environ.* 83 (1–2), 195–213. [https://doi.org/10.1016/S0034-4257\(02\)00096-2](https://doi.org/10.1016/S0034-4257(02)00096-2).
- Ichii, K., Ueyama, M., Kondo, M., Saigusa, N., Kim, J., Carmelita Alberto, M., Ardoe, J., Euskirchen, E.S., Kang, M., Hirano, T., et al., 2017. New data-driven estimation of terrestrial CO<sub>2</sub> fluxes in Asia using a standardized database of eddy covariance measurements, remote sensing data, and support vector regression. *J. Geophys. Res. Biogeosci.* 122 (4), 767–795. <https://doi.org/10.1002/2016JG003640>.
- Jeong, S.J., Ho, C.H., Gim, H.J., Brown, M.E., 2011. Phenology shifts at start vs. end of growing season in temperate vegetation over the Northern Hemisphere for the period 1982–2008. *Glob. Chang. Biol.* 17, 2385–2399. <https://doi.org/10.1111/j.1365-2486.2011.02397.x>.
- Liu, Y., Chen, Q., Ge, Q., Dai, J., Qin, Y., Dai, L., Zou, X., Chen, J., 2018b. Modelling the impacts of climate change and crop management on phenological trends of spring and winter wheat in China. *Agric. For. Meteorol.* 248, 518–526. <https://doi.org/10.1016/j.agrformet.2017.09.008>.
- Liu, Q., Fu, Y.H., Liu, Y., Janssens, I.A., Piao, S., 2018a. Simulating the onset of spring vegetation growth across the Northern Hemisphere. *Glob. Chang. Biol.* 24 (3), 1342–1356. <https://doi.org/10.1111/gcb.13954>.
- Liu, Z., Wu, C., Liu, Y., Wang, X., Fang, B., Yuan, W., Ge, Q., 2017. Spring green-up date derived from GIMMS3g and SPOT-VGT NDVI of winter wheat cropland in the North China Plain. *ISPRS J. Photogramm. Remote Sens.* 130, 81–91. <https://doi.org/10.1016/j.isprsjprs.2017.05.015>.
- Lobell, D.B., Field, C.B., 2007. Global scale climate-crop yield relationships and the impacts of recent warming. *Environ. Res. Lett.* 2 (1), 014002. <https://doi.org/10.1088/1748-9326/2/1/014002>.
- Luyssaert, S., Janssens, I., Sulkava, M., Papale, D., Dolman, A., Reichstein, M., Hollmen, J., Martin, J., Suni, T., Vesala, T., et al., 2007. Photosynthesis drives anomalies in net carbon-exchange of pine forests at different latitudes. *Glob. Chang. Biol.* 13 (10), 2110–2127. <https://doi.org/10.1111/j.1365-2486.2007.01432.x>.
- Lyapustin, A., Wang, Y., Xiong, X., Meister, G., Platnick, S., Levy, R., Franz, B., Korkin, S., Hilker, T., Tucker, J., et al., 2014. Scientific impact of MODIS C5 calibration degradation and C6+ improvements. *Atmos. Meas. Tech.* 7 (12), 4353–4365. <https://doi.org/10.5194/amt-7-4353-2014>.
- Mo, X., Liu, S., Chen, X., Hu, S., 2018. Variability, tendencies, and climate controls of terrestrial evapotranspiration and gross primary productivity in the recent decade over China. *Ecohydrology* 11 (4), e1951. <https://doi.org/10.1002/eco.1951>.
- Muraoka, H., Saigusa, N., Nasahara, K.N., Noda, H., Yoshino, J., Saitoh, T.M., Nagai, S., Murayama, S., Koizumi, H., 2010. Effects of seasonal and interannual variations in leaf photosynthesis and canopy leaf area index on gross primary production of a cool-temperate deciduous broadleaf forest in Takayama, Japan. *J. Plant Res.* 123 (4), 563–576. <https://doi.org/10.1007/s10265-009-0270-4>.
- Oldfield, E.E., Bradford, M.A., Wood, S.A., 2019. Global meta-analysis of the relationship between soil organic matter and crop yields. *Soil* 5, 15–32. <https://doi.org/10.5194/soil-5-15-2019>.
- Park, T., Ganguly, S., Tømmervik, H., Euskirchen, E.S., Høgda, K.A., Karlsen, S.R., Brovkin, V., Nemani, R.R., Myneni, R.B., 2016. Changes in growing season duration and productivity of northern vegetation inferred from long-term remote sensing data. *Environ. Res. Lett.* 11 (8), 084001. <https://doi.org/10.1088/1748-9326/11/8/084001>.
- Piao, S., Friedlingstein, P., Ciais, P., Viovy, N., Demarty, J., 2007. Growing season extension and its impact on terrestrial carbon cycle in the Northern Hemisphere over the past 2 decades. *Glob. Biogeochem. Cycles* 21 (3). <https://doi.org/10.1029/2006GB002888>.
- Piao, S., Ciais, P., Friedlingstein, P., Peylin, P., Reichstein, M., Luyssaert, S., Margolis, H., Fang, J., Barr, A., Chen, A., et al., 2008. Net carbon dioxide losses of northern ecosystems in response to autumn warming. *Nature* 451, 49–52. <https://doi.org/10.1038/nature06444>.
- Piao, S., Tan, J., Chen, A., Fu, Y.H., Ciais, P., Liu, Q., Janssens, I.A., Vicca, S., Zeng, Z., Jeong, S.J., et al., 2015. Leaf onset in the northern hemisphere triggered by daytime temperature. *Nat. Commun.* 6, 6911. <https://doi.org/10.1038/ncomms7911>.
- Piao, S., Liu, Q., Chen, A., Janssens, I.A., Fu, Y., Dai, J., Liu, L., Lian, X., Shen, M., Zhu, X., 2019. Plant phenology and global climate change: current progresses and challenges. *Glob. Chang. Biol.* 25 (6), 1922–1940. <https://doi.org/10.1111/gcb.14619>.
- Richardson, A.D., Hollinger, D.Y., Dail, D.B., Lee, J.T., Munger, J.W., O'keefe, J., 2009. Influence of spring phenology on seasonal and annual carbon balance in two contrasting New England forests. *Tree Physiol.* 29 (3), 321–331. <https://doi.org/10.1093/treephys/tpn040>.
- Richardson, A.D., Black, T.A., Ciais, P., Delbart, N., Friedl, M.A., Gobron, N., Hollinger, D.Y., Kutsch, W.L., Longdoz, B., Luyssaert, S., et al., 2010. Influence of spring and autumn phenological transitions on forest ecosystem productivity. *Philos. Trans. R. Soc. Lond. Ser. B Biol. Sci.* 365 (1555), 3227–3246. <https://doi.org/10.1098/rstb.2010.0102>.
- Rossi, S., Isabel, N., 2017. Bud break responds more strongly to daytime than nighttime temperature under asymmetric experimental warming. *Glob. Chang. Biol.* 23 (1), 446–454. <https://doi.org/10.1111/gcb.13360>.
- Schwartz, M.D., Ahas, R., Aasa, A., 2006. Onset of spring starting earlier across the Northern Hemisphere. *Glob. Chang. Biol.* 12, 343–351. <https://doi.org/10.1111/j.1365-2486.2005.01097.x>.
- Shen, M., Zhang, G., Cong, N., Wang, S., Kong, W., Piao, S., 2014. Increasing altitudinal gradient of spring vegetation phenology during the last decade on the Qinghai-Tibetan Plateau. *Agric. For. Meteorol.* 189–190, 71–80. <https://doi.org/10.1016/j.agrformet.2014.01.003>.
- Shen, M., Piao, S., Cong, N., Zhang, G., Janssens, I.A., 2015. Precipitation impacts on vegetation spring phenology on the Tibetan Plateau. *Glob. Chang. Biol.* 21 (10), 3647–3656. <https://doi.org/10.1111/gcb.12961>.
- Shen, M., Piao, S., Chen, X., An, S., Fu, Y.H., Wang, S., Cong, N., Janssens, I.A., 2016. Strong impacts of daily minimum temperature on the green-up date and summer greenness of the Tibetan Plateau. *Glob. Chang. Biol.* 22 (9), 3057–3066. <https://doi.org/10.1111/gcb.13301>.
- Sitch, S., Friedlingstein, P., Gruber, N., Jones, S.D., Murray-Tortarolo, G., Ahlstrom, A., Doney, S.C., Graven, H., Heinze, C., Huntingford, C., et al., 2015. Recent trends and drivers of regional sources and sinks of carbon dioxide. *Biogeosciences* 12 (3), 653–679. <https://doi.org/10.5194/bg-12-653-2015>.
- Tao, F., Zhang, Z., Zhang, S., Rötter, R.P., 2015. Heat stress impacts on wheat growth and yield were reduced in the Huang-Huai-Hai Plain of China in the past three decades. *Eur. J. Agron.* 71, 44–52. <https://doi.org/10.1016/j.eja.2015.08.003>.
- Wang, X., Piao, S., Xu, X., Ciais, P., MacBean, N., Myneni, R.B., Li, L., 2015. Has the advancing onset of spring vegetation green-up slowed down or changed abruptly over the last three decades? *Glob. Ecol. Biogeogr.* 24 (6), 621–631. <https://doi.org/10.1111/gcb.12289>.
- Wang, L., Zhu, H., Lin, A., Zou, L., Qin, W., Du, Q., 2017a. Evaluation of the latest MODIS GPP products across multiple biomes using global Eddy covariance flux data. *Remote Sens.* 9 (5), 418. <https://doi.org/10.3390/rs9050418>.
- Wang, S., Mo, X., Liu, Z., Baig, M.H.A., Chi, W., 2017b. Understanding long-term (1982–2013) patterns and trends in winter wheat spring green-up date over the North China Plain. *Int. J. Appl. Earth Obs. Geoinf.* 57, 235–244. <https://doi.org/10.1016/j.jag.2017.01.008>.
- Wang, H., Li, X., Ma, M., Geng, L., 2019. Improving estimation of gross primary production in dryland ecosystems by a model-data fusion approach. *Remote Sens.* 11 (3), 225. <https://doi.org/10.3390/rs11030225>.

- White, M.A., de Beurs, K.M., Didan, K., Inouye, D.W., Richardson, A.D., Jensen, O.P., O'Keefe, J., Zhang, G., Nemani, R.R., van Leeuwen, W.J.D., et al., 2009. Intercomparison, interpretation, and assessment of spring phenology in North America estimated from remote sensing for 1982–2006. *Glob. Chang. Biol.* 15 (10), 2335–2359. <https://doi.org/10.1111/j.1365-2486.2009.01910.x>.
- Wolfe, D.W., Schwartz, M.D., Lakso, A.N., Yuka, O., Pool, R.M., Shaulis, N.J., 2005. Climate change and shifts in spring phenology of three horticultural woody perennials in northeastern USA. *Int. J. Biometeorol.* 49, 303–309. <https://doi.org/10.1007/s00484-004-0248-9>.
- Wu, C., Hou, X., Peng, D., Gonsamo, A., Xu, S., 2016. Land surface phenology of China's temperate ecosystems over 1999–2013: spatial temporal patterns, interaction effects, covariation with climate and implications for productivity. *Agric. For. Meteorol.* 216, 177–187. <https://doi.org/10.1016/j.agrformet.2015.10.015>.
- Xia, J., Wan, S., 2013. Independent effects of warming and nitrogen addition on plant phenology in the Inner Mongolian steppe. *Ann. Bot.* 111 (6), 1207–1217. <https://doi.org/10.1093/aob/mct079>.
- Xia, J., Niu, S., Ciais, P., Janssens, I.A., Chen, J., Ammann, C., Arain, A., Blanken, P.D., Cescatti, A., Bonal, D., et al., 2015. Joint control of terrestrial gross primary productivity by plant phenology and physiology. *Proc. Natl. Acad. Sci.* 112 (9), 2788–2793. <https://doi.org/10.1073/pnas.1413090112>.
- Xia, H., Li, A., Feng, G., Li, Y., Qin, Y., Lei, G., Cui, Y., 2018. The effects of asymmetric diurnal warming on vegetation growth of the Tibetan Plateau over the past three decades. *Sustainability* 10 (4), 1103. <https://doi.org/10.3390/su10041103>.
- Xia, H., Qin, Y., Feng, G., Meng, Q., Cui, Y., Song, H., Ouyang, Y., Liu, G., 2019. Forest phenology dynamics to climate change and topography in a geographic and climate transition zone: the Qinling Mountains in Central China. *Forests* 10 (11), 1007. <https://doi.org/10.3390/f10111007>.
- Xiao, X., Braswell, B., Zhang, Q., Boles, S., Frolking, S., Moore III, B., 2003. Sensitivity of vegetation indices to atmospheric aerosols: continental-scale observations in Northern Asia. *Remote Sens. Environ.* 84 (3), 385–392. [https://doi.org/10.1016/S0034-4257\(02\)00129-3](https://doi.org/10.1016/S0034-4257(02)00129-3).
- Yang, F., Xu, Y., Cui, Y., Meng, Yuanduo, Dong, Y., Li, R., Ma, Y., 2017. Variation of soil organic matter content in croplands of China over the last three decades. *Acta Pedol. Sin.* 54 (5), 1047–1056. <https://doi.org/10.11766/trxb201703180633> (In Chinese).
- Yao, Y., Wang, X., Li, Y., Wang, T., Shen, M., Du, M., He, H., Li, Y., Luo, W., Ma, M., et al., 2018. Spatiotemporal pattern of gross primary productivity and its covariation with climate in China over the last thirty years. *Glob. Chang. Biol.* 24 (1), 184–196. <https://doi.org/10.1111/gcb.13830>.
- Zeng, H., Jia, G., Epstein, H., 2011. Recent changes in phenology over the northern high latitudes detected from multi-satellite data. *Environ. Res. Lett.* 6 (4), 045508. <https://doi.org/10.1088/1748-9326/6/4/045508>.
- Zhang, X., Friedl, M.A., Schaaf, C.B., Strahler, A.H., Hodges, J.C.F., Gao, F., Reed, B.C., Huete, A., 2003. Monitoring vegetation phenology using MODIS. *Remote Sens. Environ.* 84 (3), 471–475. [https://doi.org/10.1016/S0034-4257\(02\)00135-9](https://doi.org/10.1016/S0034-4257(02)00135-9).
- Zhang, G., Zhang, Y., Dong, J., Xiao, X., 2013. Green-up dates in the Tibetan Plateau have continuously advanced from 1982 to 2011. *Proc. Natl. Acad. Sci. U. S. A.* 110 (11), 4309–4314. <https://doi.org/10.1073/pnas.1210423110>.
- Zhang, H., Zhang, Y., Yan, C., Liu, E., Chen, B., 2016a. Soil nitrogen and its fractions between long-term conventional and no-tillage systems with straw retention in dryland farming in northern China. *Geoderma* 269, 138–144. <https://doi.org/10.1016/j.geoderma.2016.02.001>.
- Zhang, Z., Song, X., Tao, F., Zhang, S., Shi, W., 2016b. Climate trends and crop production in China at county scale, 1980 to 2008. *Theor. Appl. Climatol.* 123 (1–2), 291–302. <https://doi.org/10.1007/s00704-014-1343-4>.
- Zhang, Y., Xiao, X., Wu, X., Zhou, S., Zhang, G., Qin, Y., Dong, J., 2017. A global moderate resolution dataset of gross primary production of vegetation for 2000–2016. *Sci. Data* 4, 170165. <https://doi.org/10.1038/sdata.2017.165>.
- Zhang, X., Zhu, A., Xin, X., Yang, W., Zhang, J., Ding, S., 2018. Tillage and residue management for long-term wheat-maize cropping in the North China Plain: I. Crop yield and integrated soil fertility index. *Field Crop Res.* 221, 157–165. <https://doi.org/10.1016/j.fcr.2018.02.025>.
- Zhao, X., Xue, J., Zhang, X., Kong, F., Chen, F., Lal, R., Zhang, H., 2015. Stratification and storage of soil organic carbon and nitrogen as affected by tillage practices in the North China Plain. *PLoS One* 10 (6), e0128873. <https://doi.org/10.1371/journal.pone.0128873>.
- Zhao, B., Wang, X., Ata-Ul-Karim, S.T., Liu, Z., Duan, A., 2019. Effect of straw incorporation on corn yield in North China: a meta-analysis. *J. Biobased Mater. Bioenergy* 13 (4), 532–536. <https://doi.org/10.1166/jbmb.2019.1872>.
- Zhou, S., Zhang, Y., Caylor, K.K., Luo, Y., Xiao, X., Ciais, P., Huang, Y., Wang, G., 2016. Explaining inter-annual variability of gross primary productivity from plant phenology and physiology. *Agric. For. Meteorol.* 226–227, 246–256. <https://doi.org/10.1016/j.agrformet.2016.06.010>.
- Zhou, S., Zhang, Y., Ciais, P., Xiao, X., Luo, Y., Caylor, K.K., Huang, Y., Wang, G., 2017. Dominant role of plant physiology in trend and variability of gross primary productivity in North America. *Sci. Rep.* 7, 41366. <https://doi.org/10.1038/srep41366>.
- Zhu, W., Tian, H., Xu, X., Pan, Y., Chen, G., Lin, W., 2012. Extension of the growing season due to delayed autumn over mid and high latitudes in North America during 1982–2006. *Glob. Ecol. Biogeogr.* 21 (2), 260–271. <https://doi.org/10.1111/j.1466-8238.2011.00675.x>.
- Zhu, X., Yu, G., He, H., Wang, Q., Chen, Z., Gao, Y., Zhang, Y., Zhang, J., Yan, J., Wang, H., et al., 2014. Geographical statistical assessments of carbon fluxes in terrestrial ecosystems of China: results from upscaling network observations. *Glob. Planet. Chang.* 118, 52–61. <https://doi.org/10.1016/j.gloplacha.2014.04.003>.
- Zhu, H., Lin, A., Wang, L., Xia, Y., Zou, L., 2016. Evaluation of MODIS gross primary production across multiple biomes in China using Eddy covariance flux data. *Remote Sens.* 8 (5), 395. <https://doi.org/10.3390/rs8050395>.
- Zohner, C.M., Benito, B.M., Svenning, J.C., Renner, S.S., 2016. Day length unlikely to constrain climate-driven shifts in leaf-out times of northern woody plants. *Nat. Clim. Chang.* 6, 1120–1123. <https://doi.org/10.1038/nclimate3138>.